



This is a repository copy of *Sensorimotor processing in the basal ganglia leads to transient beta oscillations during behavior*.

White Rose Research Online URL for this paper:
<http://eprints.whiterose.ac.uk/121321/>

Version: Accepted Version

Article:

Mirzaei, A., Kumar, A., Leventhal, D. et al. (4 more authors) (2017) Sensorimotor processing in the basal ganglia leads to transient beta oscillations during behavior. *The Journal of Neuroscience*, 37 (46). pp. 11220-11232. ISSN 0270-6474

<https://doi.org/10.1523/JNEUROSCI.1289-17.2017>

Reuse

Items deposited in White Rose Research Online are protected by copyright, with all rights reserved unless indicated otherwise. They may be downloaded and/or printed for private study, or other acts as permitted by national copyright laws. The publisher or other rights holders may allow further reproduction and re-use of the full text version. This is indicated by the licence information on the White Rose Research Online record for the item.

Takedown

If you consider content in White Rose Research Online to be in breach of UK law, please notify us by emailing eprints@whiterose.ac.uk including the URL of the record and the reason for the withdrawal request.



eprints@whiterose.ac.uk
<https://eprints.whiterose.ac.uk/>

1 **Sensorimotor processing in the basal ganglia leads** 2 **to transient beta oscillations during behavior**

3 **Authors (ordered):**

4 Amin Mirzaei^{1,2}, Arvind Kumar^{3,4}, Daniel Leventhal⁵, Nicolas Mallet⁶, Ad Aertsen^{2,4}, Joshua
5 Berke⁷, Robert Schmidt⁸.

6 ¹BrainLinks-BrainTools, University of Freiburg, Freiburg, Germany.

7 ²Faculty of Biology, University of Freiburg, Freiburg, Germany.

8 ³Computational Biology, School of Computer Science and Communication, KTH Royal Institute
9 of Technology, Stockholm, Sweden.

10 ⁴Bernstein Center Freiburg, University of Freiburg, Freiburg, Germany.

11 ⁵Department of Neurology, University of Michigan, Ann Arbor, MI 48109, United States.

12 ⁶Universite de Bordeaux, Institut des Maladies Neurodegeneratives, 33076 Bordeaux, France.

13 ⁷Department of Neurology and Kavli Institute for Fundamental Neuroscience, University of
14 California San Francisco, USA.

15 ⁸Department of Psychology, University of Sheffield, UK.

16 **Corresponding author:** Correspondence should be addressed to Amin Mirzaei, Faculty of
17 Biology, University of Freiburg, Hansastrasse 9a, 79104 Freiburg, Germany.

18 Email: amin.mirzaei@brainlinks-braintools.uni-freiburg.de

19 **Number of pages:** 27

20 **Number of figures:** 8

21 **Number of words for Abstract:** 206

22 **Number of words for Introduction:** 651

23 **Number of words for Discussion:** 1648

24 **Acknowledgments:**

25 We thank Wei Wei, Alejandro Jimenez, Lars Hunger, and Mohammad Mohagheghi Nejad for
26 useful comments and discussion. This work was supported by BrainLinks-BrainTools Cluster of
27 Excellence funded by the German Research Foundation (DFG, grant number: EXC 1086) and the
28 University of Sheffield. We also acknowledge support by the state of Baden-Württemberg through
29 bwHPC and the German Research Foundation (DFG) through grant no INST 39/963-1 FUGG.

Abstract

Brief epochs of beta oscillations have been implicated in sensorimotor control in the basal ganglia of task-performing healthy animals. However, which neural processes underlie their generation and how they are affected by sensorimotor processing remains unclear. To determine the mechanisms underlying transient beta oscillations in the local field potential (LFP), we combined computational modeling of the subthalamo-pallidal network for the generation of beta oscillations with realistic stimulation patterns derived from single unit data. The single unit data were recorded from different basal ganglia subregions in rats performing a cued choice task. In the recordings we found distinct firing patterns in the striatum, globus pallidus and subthalamic nucleus related to sensory and motor events during the behavioral task. Using these firing patterns to generate realistic inputs to our network model lead to transient beta oscillations with the same time course as the rat LFP data. In addition, our model can account for further non-intuitive aspects of beta modulation, including beta phase resets following sensory cues and correlations with reaction time. Overall, our model can explain how the combination of temporally regulated sensory responses of the subthalamic nucleus, ramping activity of the subthalamic nucleus, and movement-related activity of the globus pallidus, leads to transient beta oscillations during behavior.

Significance Statement

Transient beta oscillations emerge in the normal functioning cortico-basal ganglia loop during behavior. In this work we employ a unique approach connecting a computational model closely with experimental data. In this way we achieve a simulation environment for our model that mimics natural input patterns in awake behaving animals. Using this approach we demonstrate that a computational model for beta oscillations in Parkinson’s disease can also account for complex patterns of transient beta oscillations in healthy animals. Therefore, we propose that transient beta oscillations in healthy animals share the same mechanism with pathological beta oscillations in Parkinson’s disease. This important result connects functional and pathological roles of beta oscillations in the basal ganglia.

Introduction

Exaggerated cortico-basal ganglia oscillations in the beta band (15 to 30 Hz) are a common feature of Parkinson’s disease (PD; Brown et al., 2001; Hammond et al., 2007; Levy et al., 2002). However, beta oscillations are not always pathological. Brief epochs of beta oscillations have been implicated in sensorimotor control in the healthy basal ganglia (Berke et al., 2004; Leventhal et al., 2012; Courtemanche et al., 2003; Feingold et al., 2015). These studies suggest that temporally regulated transient beta oscillations are important for normal functioning of the motor system.

The origin of beta oscillations in the cortico-basal ganglia system remains unknown. However, interactions between subthalamic nucleus (STN) and globus pallidus externa (GPe) can generate beta oscillations as has been shown in experimental (Bevan et al., 2002; Tachibana et al., 2011) and computational (Terman et al., 2002; Kumar et al., 2011, Pavlides et al., 2015; Wei et al., 2015) studies. Anatomically, STN and GPe are densely and reciprocally inter-connected (Shink et al., 1996). STN cells excite neurons in GPe (Kitai and Kita, 1987), which in turn receive inhibitory

69 input from GPe (Smith et al., 1990; Parent and Hazrati, 1995). Such recurrent excitation-inhibition
70 can generate oscillations (Plenz and Kitai, 1999; Brunel, 2000), which may then propagate to other
71 regions in the cortico-basal ganglia loop.

72 Beta oscillations have been proposed to play a functional role in maintaining the status quo in
73 the motor system (Engel and Fries, 2010; Gillbertson et al., 2005). This idea has been supported
74 by increased cortical beta-band activity during maintenance of a static position (Baker et al.,
75 1997), active suppression of movement initiation (Swann et al., 2009), and post-movement hold
76 periods (Pfurtscheller et al., 1996). Accordingly, beta power decreases in the cortico-basal ganglia
77 loop during movement preparation and execution (Sochurkova and Rektor, 2003; Pfurtscheller et
78 al., 2003; Alegre et al., 2005; Kuhn et al., 2004). However, recent studies have indicated a more
79 complex picture in which beta oscillations affect behavior through motor adaptation (Tan et al.,
80 2014) and modulation of task performance (Feingold et al., 2015).

81 Supporting a more complex picture of beta oscillations, we provided evidence that basal ganglia
82 beta oscillations are involved in sensorimotor processing and the utilization of cues for behavior
83 (Leventhal et al., 2012). In particular, we found that beta power increases following sensory cues
84 and movement initiation depended on how fast the animals reacted to a sensory cue. For short
85 reaction times, LFP beta emerged after movement initiation, whereas for long reaction times,
86 two separate beta epochs occurred, one before and one after movement initiation. In addition
87 to modulation of beta power, we also observed that beta phases were affected by task events
88 differently. Sensory cues, but not movement initiation, lead to a short-latency phase reset in the
89 beta band (Leventhal et al., 2012).

90 These complex oscillatory dynamics present both a challenge, and an opportunity, for under-
91 standing underlying cortico-basal ganglia circuit mechanisms. Currently, it is unknown whether
92 pathological beta oscillations in Parkinson’s disease share the same mechanisms with transient
93 beta oscillations in healthy animals. If this is the case, computational models for beta oscillations
94 should be able to account for the complex beta dynamics in both healthy and Parkinsonian animals.
95 Recent network models of beta oscillations in Parkinson’s disease have emphasized that besides
96 structural changes (e.g. connection strengths), changes in spiking activity of external inputs can
97 promote beta oscillations (Kumar et al., 2011), which might drive transient beta oscillations. Here
98 we exploit this property by directly using activity patterns recorded in healthy rats during task
99 performance (Schmidt et al., 2013; Mallet et al., 2016) as input to our computational model to
100 study the resulting impact on the beta dynamics. Employing this novel approach we find that our
101 model can account for the complex beta dynamics in the healthy rat LFP. Our results support
102 overlapping mechanisms for pathological and healthy beta oscillations and provide the basis for
103 studying the functional role of beta oscillations in network models.

104 **Materials and methods**

105 *Network model.* The basic model structure and the parameter settings are the same as in Kumar
106 et al. (2011). Briefly, the model includes 1000 excitatory STN neurons, and 2000 inhibitory GPe
107 neurons. Neurons were implemented as leaky integrate-and-fire neurons. Synaptic input was
108 modeled as transient exponential conductance changes. All model neurons receive uncorrelated
109 Poisson spike trains as inputs so as to achieve previously reported baseline activities for STN (15
110 Hz) and for GPe (45 Hz; Bergman et al., 1994; Raz et al., 2000). All network simulations were

111 written in python using pyNN as an interface to the simulation environment NEST (Gewaltig
 112 and Diesmann, 2007). Analysis of the simulation results and the LFP and single unit data were
 113 performed using MATLAB R2013b (version 8.2.0.701; The MathWorks Inc., Natick, MA).

114 For the model variant without recurrent connections in STN (Figure 8), we used slightly different
 115 parameters for the connection probabilities, synaptic weights and transmission delays (Table 1).
 116 Furthermore, the background Poisson input to the model neurons was adjusted so that the neurons
 117 had a broader distribution of baseline firing rates that closer matched the firing rate distribution
 118 in the rat data (Schmidt et al., 2013; Mallet et al., 2016).

Table 1: Comparison of model parameters in Kumar et al. (2011) and the modified model without recurrent STN connections.

Kumar et al., 2011	Modified model
$CP_{STN-STN} = 0.02$	$CP_{STN-STN} = 0$
$CP_{STN-GPe} = 0.02$	$CP_{STN-GPe} = 0.022$
$CP_{GPe-STN} = 0.02$	$CP_{GPe-STN} = 0.035$
$CP_{GPe-GPe} = 0.02$	$Cp_{GPe-GPe} = 0.02$
$J_{STN-STN} = 1.2$	$J_{STN-STN} = -$
$J_{STN-GPe} = 1.2$	$J_{STN-GPe} = 1.2$
$J_{GPe-STN} = -1.135$	$J_{GPe-STN} = -0.8$
$J_{GPe-GPe} = -0.725$	$J_{GPe-GPe} = -0.725$
$d_{STN-STN} = 2$	$d_{STN-STN} = -$
$d_{STN-GPe} = 5$	$d_{STN-GPe} = 6$
$d_{GPe-STN} = 5$	$d_{GPe-STN} = 6$
$d_{GPe-GPe} = 2$	$d_{GPe-GPe} = 3$

CP: Connection Probability, J: Synaptic weight, d: Delay (in ms)

119 *Experimental design and statistical analysis.* We combined previously recorded data sets of
 120 tetrode recordings in different basal ganglia subregions of rats performing a stop-signal task (for
 121 details see Leventhal et al., 2012; Schmidt et al., 2013; Mallet et al., 2016). To exclude potential
 122 multi-unit activity from our recordings, we only included units with less than 1% of inter spike
 123 intervals shorter than 1 ms in our data set. The combined data set contained 226 STN units
 124 from overall 40 recording sessions in 5 different rats, 149 putative prototypical GPe units from
 125 41 recording sessions in 4 different rats, and 326 putative MSNs from 97 recording sessions in 9
 126 different rats. Between two recording sessions tetrodes were typically moved by at least $80\mu\text{m}$, and
 127 we therefore considered units recorded in different sessions as different units. Animals performed
 128 a stop-signal task, but here we only analyzed the subset of correct Go trials in which the animal
 129 moved contralateral to the recording site.

130 To identify STN neurons responding to the Go cue instructing contralateral movement (Figures
 131 1C, D), we used a shuffle test to determine whether neural activity significantly increased within

132 150 ms after the Go cue. The time of each spike within -500 ms to +200 ms relative to the Go cue
133 was changed to a random spike time within the same time window. Then we compared the number
134 of actual spikes with the number of shuffled spikes in small time windows after the Go cue (15
135 non-overlapping 10 ms windows from 0 to 150 ms after the Go cue). We repeated this procedure
136 10000 times and used the fraction of shuffles in which the number of shuffled spikes exceeded the
137 number of actual spikes as the p-value to estimate statistical significance. STN neurons showing
138 a p-value less than 0.05/15 for at least one bin after the time of the Go cue were considered
139 sensory responsive. We performed the same shuffling method on GPe neurons to select movement
140 responsive GPe neurons (Figure 1F), using all spikes within -1s to +1s relative to movement onset
141 to detect firing rate changes for 50 ms time windows from 0 to 250 ms after movement onset (i.e.
142 5 non-overlapping time bins). GPe neurons showing a p-value less than 0.05/5 for at least one bin
143 after movement onset were considered as movement responsive.

144 To identify movement-responsive MSNs in our single unit data, average firing rates of MSNs
145 were sorted based on their peak time within the interval from one second before to one second
146 after movement initiation. MSNs with a peak firing rate between 150 ms before to 150 ms after
147 movement onset were considered as movement-responsive MSNs (n = 100; see Figure 1E).

148 To determine whether a recorded unit showed a ramping firing pattern, we computed the average
149 firing rates of each unit from one subregion over trials with a 50 ms sliding time window moving
150 in steps of 10 ms from 1 s before the time of Go cue to the time of Go cue. Each resulting
151 average firing rate was then normalized to values between 0 and 1 and then mean-subtracted
152 before applying principal component analysis. First, we computed the corresponding covariance
153 matrix of all normalized zero-mean firing rates. and then performed eigendecomposition on the
154 covariance matrix using the *eig* function of MATLAB. The projection p of each normalized zero-
155 mean average firing rate r to the first eigenvector (corresponding to the maximum eigenvalue) was
156 then computed as the normalized dot product: $p_i = \langle r_i, v_1 \rangle / \lambda_1$, where i is the unit index and v_1 the
157 eigenvector with the largest eigenvalue λ_1 . This yielded one projection value p_i for each recorded
158 unit. As the first eigenvector had a positive ramp over time, positive and negative projection values
159 corresponded to positive and negative activity ramps of a recorded unit over time, respectively.
160 The standard deviation of the projection distribution from a random covariance matrix is $1/\sqrt{n}$
161 (Anderson, 2003), with n being the number of units. We considered neurons with a projection
162 larger than $2/\sqrt{n}$ or smaller than $-2/\sqrt{n}$ as positive and negative ramp neurons, respectively
163 (Figures 2A, B). This analysis method was applied to determine positive and negative ramps in
164 GPe and STN.

165 *Modeling of sensory responses.* To simulate sensory responses of STN neurons to the Go cue
166 (Figures 1C, D), we used inhomogeneous Poisson generators, each of which targeted one STN
167 neuron in the model. The firing rate modulation of each inhomogeneous Poisson generator was a
168 half sine wave with a duration of 20 ms and maximum amplitude of 180 Hz. The latency of the
169 sensory stimulation for each STN neuron in the model was considered as the time interval between
170 the peak of the half sine wave and the time of the Go cue, which was taken randomly from the
171 latency distribution of the sensory STN neurons in our experimental data (Figure 1D). Since in
172 our single unit data 30% of the STN neurons responded to the Go cue, for each simulation we
173 targeted 30% of randomly chosen STN neurons (as “sensory” STN neurons) in the network model.
174 Thereby, sensory responses in STN neurons could propagate in our network model to GPe, similar
175 to some short latency responses we previously reported in GPe (Schmidt et al.,2013).

176 *Modeling of motor responses.* Firing rates of the movement-responsive MSNs (Figure 1E) were
177 summed up and used as the firing rate pattern of an inhomogeneous Poisson generator representing
178 striato-pallidal movement-related inhibition in the network model. Since 38% of the GPe neurons
179 in our experimental data showed movement-related inhibition (Figure 1F), for each simulation we
180 targeted a randomly chosen 38% of the GPe neurons (as “motor” GPe neurons) in the network
181 model.

182 *Modeling of firing rate ramps.* To simulate the positive and negative ramps in the activity of
183 the STN neurons observed before the Go cue (Figures 2A, B), for each simulation, we divided
184 STN neurons in the network model into two non-overlapping subpopulations. The fraction of STN
185 neurons in each subpopulation in the network model was similar to the fraction we obtained from
186 our experimental data (i.e. 34% of neurons exhibited a positive ramp, 43% a negative ramp). We
187 used an inhomogeneous Poisson generator with a positive ramp firing rate pattern as excitatory
188 input to the positive ramp STN subpopulation in the model. The positive ramp in the firing rate
189 of the inhomogeneous Poisson generator started 500 ms before the Go cue at 0 Hz and reached 250
190 Hz at the time of the Go cue and stayed constant until the movement onset (Figure 3B). Such a
191 stimulation lead to a 4 Hz increase in the activity of the positive ramp STN subpopulation in the
192 network model during the 500 ms time interval preceding the Go cue, similar to what we observed
193 in our experimental data (Figure 2A).

194 Similarly, to simulate the negative ramp in the activity of STN neurons, we used another
195 inhomogeneous Poisson generator with a positive ramp firing rate pattern as inhibitory input to
196 the negative ramp STN model neuron subpopulation. The positive ramp in the firing rate of the
197 inhibitory inhomogeneous Poisson generator started 500 ms before the time of Go cue at 0 Hz and
198 reached 350 Hz at the time of the Go cue and stayed constant until the movement onset. Such a
199 stimulation pattern lead to a 1 Hz decrease in the activity of the negative ramp STN neurons in
200 the network model during 500 ms time interval preceding the Go cue, similar to what we observed
201 in our experimental data (Figure 2B).

202 *Time-frequency analysis.* The power spectrogram was computed by convolving 10 seconds of the
203 GPe population firing rate (from -5 to +5 seconds relative to the time of movement onset) in the
204 model with a standard Morlet wavelet ($\sigma = 0.849/f$) of integer frequencies ($f = 1$ to 500 Hz),
205 and taking the logarithm of the squared magnitude of the resulting time series. To generate Figure
206 3C, bottom, we computed the mean spectrogram across 400 simulations of the model. The same
207 method was used for GPe LFP data to generate Figure 3C, top. For each time point in the
208 spectrogram, we summed the power in the beta range (15 to 30 Hz) and divided it by the summed
209 power across all frequencies (1 to 500 Hz) to obtain continuous relative beta power, shown in
210 Figures 4A, 4B, 4E, 4F, and 6B.

211 *Mean resultant length.* The GPe population firing rate in the network model was convolved with
212 the standard Morlet wavelet of each integer frequency in the beta band (15 to 30 Hz). For each
213 frequency, the Hilbert transform of the filtered signal was computed to obtain a phase over time.
214 The phase spread for each time point was then calculated by computing the length of the mean
215 resultant vector over all trials using $MRL(t) = \frac{1}{n} \sum_n e^{i\theta(n,t)}$, where $\theta(n,t)$ is the phase of the n th
216 trial at time t ($n = 400$ for the model). This results in a continuous measure of phase spread for
217 each frequency in the beta range. The mean resultant lengths shown in Figure 4 were computed
218 by taking the average across all beta frequencies.

Results

To determine whether a computational model for pathological beta oscillations in the STN-GPe network (Kumar et al., 2011) can account for complex beta dynamics during behavior in healthy animals, we devised realistic stimulation patterns for the network model based on single unit recordings in rats performing a cued choice task (Schmidt et al., 2013; Mallet et al., 2016). At the beginning of each trial, the rat entered one of three center nose ports in an operant chamber (“Nose-in” event; Figures 1A, B). The rat was trained to then hold its position for a variable time interval (“Holding time”; 500-1200 ms) until a Go cue instructed the rat to quickly move its head to the adjacent left or right side port (“Nose-out” event; Figures 1A, B). Correct performance of the task was rewarded with a sugar pellet. While the animals performed the task we recorded in the striatum, GPe and STN to determine activity patterns of single units during the time of the Go cue and during movement initiation. Then we used these activity patterns to construct realistic input patterns for our network model. The network model we use here is a large-scale spiking network model consisting STN and GPe populations with conductance based synapses (Kumar et al., 2011; see Methods). Stimulating the network model via the realistic stimulation patterns allowed us to compare the resulting oscillatory dynamics in the model with properties of oscillations in the rat LFPs.

Brief, short-latency sensory responses in STN. 30% (70/226) of STN units responded to the Go cue with an increase in firing rate (Figure 1C; shuffle test, $p < 0.05/15$; see Methods). In line with our previous reports on a subset of the same data (Schmidt et al., 2013), this included units with a very short latency (around 10-30 ms), and responses of individual units were typically very brief (see Figure 1C, top panel). A potential source of such short latency sensory responses of the STN units is pedunclopontine tegmental nucleus (PPN; Pan and Hyland, 2005). In addition to the short latency responses of the STN units, some STN units responded with a longer latency (around 40-100 ms), so that the overall distribution of peak response latencies had a bimodal shape (Figure 1D). To mimic this STN response pattern to salient sensory stimuli, individual STN units received brief excitatory pulses with a fixed latency sampled from the latency distribution. These pulses were then used as input to 30% randomly chosen STN model neurons (“sensory” STN neurons) to match the fraction of responding STN units in our single unit data.

Movement-related activity in striatum and GPe. 30% (100/320) of putative medium spiny neurons (MSNs) in the striatum increased their activity during contralateral movements (Figure 1E; see Methods; also see Schmidt et al., 2013). We focused here on contralateral movements as most neurons typically responded more during contralateral than ipsilateral movements (Gage et al., 2010; Schmidt et al., 2013). In GPe, 38% (56/149) of the units decreased their activity during contralateral movements (Figure 1F; shuffle test, $p < 0.05/5$; see Methods), possibly reflecting input from indirect pathway MSNs. Therefore, we assumed in the network model that striato-pallidal inhibition drives the GPe firing rate decreases during movement. We implemented this by generating inhomogeneous Poisson spike trains with a rate modulation following the MSN firing pattern during movement (Figure 1E). These spike trains were then used as inhibitory inputs to 38% of the network model GPe neurons (“motor” GPe neurons) to match the fraction of GPe units with movement-related firing rate decreases in the single unit data. Note that we restricted our analysis of GPe units to putative prototypical neurons (Mallet et al., 2016) because they receive input from MSNs and project to STN, while arkypallidal GPe neurons probably receive different inputs and do not project to STN (Mallet et al., 2012; Dodson et al., 2015).

263 *Ramping activity in STN and GPe while rats wait for the Go cue.* In addition to single unit
264 responses that could be classified as sensory or motor, in STN and GPe we found many units
265 which exhibited a firing pattern that resembled a “ramp”, a continuous change in firing rate.
266 A ramping pattern was present in the activity of 77% (176/226) of the STN units with either
267 significantly increasing (positive ramp) or decreasing (negative ramp) firing rate while the animal
268 was waiting for the Go cue (Figures 2A, B). Among the 176 ramping STN units, 44% (78/176)
269 showed positive ramps (Figure 2A), whereas 55% (98/176) showed negative ramps (Figure 2B).
270 However, the mean firing rate increase for the positive ramp units was four times as high as the
271 mean firing rate decrease for the negative ramp units (4 Hz increase vs. 1 Hz decrease; inset in
272 Figure 2B, bottom). The positive ramp was also observed in the average firing rate of the whole
273 STN population starting 500 ms before the Go cue (data not shown). Functionally, these ramps
274 may correspond to a brake signal, preventing premature movement initiation (Frank, 2006).

275 We found a similar pattern in the GPe with 71% (106/149) of the units exhibiting a significant
276 ramping activity before the Go cue (Figures 2C, D). Among these, 47% (50/106) showed positive
277 ramps (Figure 2C) and 52% showed negative ramps (Figure 2D). Similar to the STN units, on
278 average, the amplitude of the positive ramp in GPe was four times as high as the amplitude of
279 the negative ramp, resulting in a net positive ramp in the population activity (data not shown).
280 One property of the positive ramp STN and GPe units was that in long reaction time trials their
281 activity remained elevated after the Go cue (Figures 2A, C, bottom panels). This property played
282 a key role for the beta dynamics in the model below.

283 Based on these ramping patterns in STN and GPe, we designed inputs to the model STN
284 neurons that lead to similar activity ramps (see Methods). Due to the excitatory drive from STN
285 to GPe, in the model the ramps in STN activity resulted in corresponding ramps in GPe.

286 *Sensorimotor model inputs modulate time course of beta oscillations.* As a previous modeling
287 study demonstrated that excitatory input to STN or inhibitory input to GPe can induce transient
288 beta oscillations (Kumar et al., 2011), we hypothesized that the sequence of ramp, Go cue and
289 movement-related activity patterns (Figures 3A, B) accounts for the complex beta dynamics in
290 the LFP (Leventhal et al., 2012). First, we reproduced the time course of beta power modulation
291 during movement initiation (Leventhal et al., 2012) using an extended data set of GPe recordings
292 (Schmidt et al., 2013; Mallet et al., 2016). In the rat LFPs beta power started to increase before
293 the time of movement initiation and then showed a pronounced peak just after movement onset
294 (Figure 3C, top). The time course of beta power in the network model exposed to our single-unit
295 stimulation patterns (Figure 3B) matched the experimentally observed results (Figure 3C, bottom),
296 including the pre-movement beta power increase, the pronounced beta peak during movement, and
297 the second beta peak related to the movement out of the side port (see Methods). The network
298 model beta time course was in this case determined by the STN ramping activity, combined
299 with the sensory responses of the STN neurons and the striato-pallidal motor inputs (Figure 3B).
300 This is an important result because it connects single unit activity during task performance with
301 oscillatory network dynamics.

302 Here we compared the experimental LFP data with the model population firing rate (Figure
303 3C). However, the origin of the LFP and its relation to spiking activity are not well understood in
304 the basal ganglia. It seems that the LFP mostly reflects synchronized postsynaptic currents (Niedermeier
305 and Lopez da Silva, 1998; Nunez and Srinivasan, 2005; Jensen et al., 2005; McCarthy et
306 al., 2011). However, we found that the time course of beta oscillations was very similar, irrespec-

307 tive of whether we used the population firing rate or the summation of inhibitory or excitatory
308 postsynaptic currents to represent the experimental LFP data (data not shown). Therefore, to stay
309 consistent with previous models (e.g. Kumar et al., 2011; Pavlides et al., 2015; Nevado-Holgado
310 et al., 2014) we continue to use the population firing rate in the model to determine the presence
311 of beta oscillations.

312 *Sensory responses in STN lead to a beta phase reset.* In addition to the described changes in
313 beta power, the phases of beta oscillations can be modulated by specific events in the behavioral
314 task. Sensory cues (like the auditory Go cue) that did not lead to a distinctive increase in beta
315 power were nevertheless followed by a short-latency phase reset in the LFP (Leventhal et al.,
316 2012). By contrast, beta power increases during movement were not accompanied by a phase
317 reset in the beta band (Leventhal et al., 2012). Here, we confirm this result for GPe recording
318 sites using an extended data set (Figures 4A, E; Schmidt et al., 2013; Mallet et al., 2016). To
319 determine which properties of the neural signal lead to a phase reset or to a power increase in the
320 beta band, we calculated grand averages of raw LFP traces (Figure 4C). We found that briefly
321 after the Go cue a single beta cycle was visible. This short oscillation was rather weak and could
322 only be visible when looking at the mean of the LFP data over many trials (Figure 4C). This
323 brief beta epoch was associated with beta phase reset in the LFP data, following the Go cue
324 (Figure 4A). Interestingly, providing brief stimulation to the “sensory” STN neurons in the model
325 leads to a brief low-amplitude beta oscillation, which also only became visible when inspecting
326 the mean population firing rate over many stimulations (Figure 4D). Similar to the experimental
327 data, “sensory” stimulation of the model STN leads to beta phase reset in the ongoing activity
328 of the network model (Figure 4B). Therefore, we conclude that brief excitatory inputs to STN
329 can induce weak and brief, phase-locked beta oscillations in the STN-GPe network, mimicking the
330 experimentally observed results.

331 Beta elevation around the time of movement onset was not accompanied by a phase reset in both
332 the rat LFP data and in the model (Figures 4E, F). It might seem counterintuitive that a strong
333 stimulation leading to a clear increase in beta power did not reset the phase, whereas a weaker
334 stimulation did. However, STN neuronal responses to the Go cue are brief, compared to the longer
335 movement-related increases in the activity of MSNs (Figures 1C-E). Therefore, we hypothesized
336 that the duration of neural responses to sensory and motor events might be the key difference. To
337 test this, we systematically varied the duration of the inputs to the model “sensory” STN neurons
338 and “motor” GPe neurons (note that the inputs are inhomogeneous Poisson spike trains with firing
339 rate patterns of a half cosine wave; see Methods). We found that for brief inputs (leading to brief
340 changes in the neuronal activity) there was a phase reset in the ongoing activity of the network
341 model (Figure 5). Longer stimulations of “motor” GPe neurons elevated the beta power without
342 phase reset (Figures 5C, D). For stimulation durations longer than a single beta period in the model
343 (i.e. about 50 ms), we only observed beta power elevation without phase reset (Figures 5C, D). In
344 fact, the maximal phase reset in the network model occurred when the stimulation duration was
345 25 ms, equaling half the beta cycle (Figures 5B, D). For the short stimulation duration the time to
346 get to the maximum of the half cosine firing rate pattern is short (i.e. the slope is steeper). This
347 effectively leads to no trial-to-trial variability because all realizations of the Poisson process with
348 such a brief firing rate pattern are very similar (with respect to the spike times). This similarity
349 in the input then leads to a similar response in the network model and therefore a phase reset
350 across trials. In contrast, for longer stimulation the time to get to the maximum of the half cosine
351 firing rate pattern is longer (with shallower slope). This leads to more trial-to-trial variability
352 with respect to the spike times in the realization of the Poisson process. Correspondingly, this

353 translates into trial-to-trial variability in the response of the network model to the long stimulation
354 and therefore a random phase across trials.

355 Longer stimulations of the “sensory” STN neurons did not elevate the beta power in the network
356 model (Figure 5A). This is because “sensory” STN units made up a smaller fraction (30%) of
357 the STN population in our model compared to 38% “motor” GPe units (see above). The long
358 stimulation of a small fraction of the STN neurons was not sufficient to bring the network model
359 into the oscillatory state. In general, for a certain stimulation strength, the fraction of stimulated
360 neurons in the network model is a key parameter determining the amount of evoked beta power
361 (Kumar et al., 2011).

362 *Disentangling the complex relationship between reaction time and beta dynamics.* The time
363 course of beta oscillations depends on how fast the animal initiates movement in response to the
364 Go cue (Leventhal et al., 2012). For short reaction times, the mean LFP beta power shows a single
365 peak after movement initiation. For long reaction times, the mean LFP beta power shows two
366 peaks, with the first peak before and the second peak after movement initiation (see highlighted
367 300 ms epochs preceding and following Nose Out in Figure 6A, right; see also Leventhal et al.,
368 2012). The bimodal shape of the mean beta power for long reaction time trials is also visible when
369 aligned to the Go cue (Figure 6A, left). A straightforward idea would be that the first peak of the
370 mean beta power for long reaction time trials is mostly driven by the Go cue or, alternatively, by
371 the upcoming movement. However, if the beta peak was driven by the Go cue, we would expect
372 a higher peak for the data aligned to the Go cue than for the data aligned to movement onset.
373 Accordingly, if the beta peak was related to the movement, we would instead expect a higher
374 peak for the data aligned to the movement onset. In contrast, despite variability in reaction time,
375 this peak had a similar shape and amplitude for both alignment to the Go cue and to movement
376 onset. Therefore, this beta peak does not seem to be simply driven by a sensory or motor event.
377 With the help of our network model, we disentangle the mechanisms underlying these reaction
378 time-dependent complex features of beta.

379 Using our stimulation patterns based on single unit recordings, we studied how different reaction
380 times affect the time course of beta power. We found a strikingly similar effect of reaction time
381 on the time course of beta power in the network model (Figure 6B). For long reaction time trials
382 the model exhibited two separate peaks in the mean beta power with the same time course as the
383 experimental LFP data (Figure 6B). Furthermore, the peak of the mean beta power in the model
384 after movement onset for short reaction time trials had a higher amplitude than in long reaction
385 time trials, similar to the experimental LFP data (see right panels in Figures 6A and 6B). The
386 ability of the model to capture the fine details of the complex beta power modulation became
387 visible even at the single-trial level (Figures 6C, D). As in the experimental data, changes in mean
388 power modulation were reflected as a change in the probability of a transient beta oscillation,
389 rather than as only a gradual increase in the oscillation amplitude.

390 To understand the mechanisms underlying the complex relationship between beta and reaction
391 times, we can now use our network model to determine the contribution of each stimulation
392 component. Before the Go cue, ramping activity of the STN neurons in the model causes a
393 gradual increase in beta power (mostly because of an increase in the probability of a beta event),
394 starting almost 600 ms before the Go cue (Figures 6B, D and Figure 7). At the time of the Go cue
395 the sensory responses of the STN neurons generate a weak and brief beta oscillation in the model
396 (green traces in Figure 7). In short reaction time trials this brief beta oscillation overlaps with beta

397 oscillations driven by “ramp” and “motor” inputs (as sensory and motor events are temporally
398 close). This overlap results in an interaction of ongoing beta (driven by “ramp” input) with beta
399 driven by “motor” input, leading to high beta power around the time of movement onset (Figures
400 6B and 7, top). For long reaction time trials, after the Go cue, but before movement initiation, the
401 “sensory” and “ramp” inputs determine the beta dynamics in the model. The interaction between
402 the “sensory” and “ramp” inputs leads to the first, high-amplitude beta peak for long reaction
403 time trials (Figures 6B and 7, bottom). As Go cue and Nose Out events are temporally distant
404 for long trials, this high-amplitude beta power starts to decay before the time of movement onset.
405 This is followed by another beta epoch due to “motor” input which leads to the second peak of
406 beta power, after the time of movement onset, for long reaction time trials (Figures 6B, D and
407 7). The amplitude of this second peak is smaller, compared to the peak after movement onset for
408 short reaction time trials (Figure 6B, right), because it lacks the interaction with STN excitation
409 due to the Go cue (Figure 7). Functionally, the first beta peak in long reaction time trials may be
410 linked to the prolongation of movement initiation in high beta states (Levy et al., 2002; Brown et
411 al., 2001; Chen et al., 2007; Pogosyan et al., 2009). Thereby our model connects “ramp” activity
412 in STN with the generation of beta oscillations and potential functional roles as a “brake” (Frank,
413 2006).

414 *Our results are robust to the STN-STN recurrent connectivity in the network model.* In the
415 network model we used, the STN neurons received excitatory synaptic inputs from other STN
416 neurons with a connection probability of 2% (Kumar et al., 2011). However, several experimental
417 studies indicate that the STN-STN recurrent connectivity is very rare or do not exist (Hamond
418 and Yelnik, 1983; Sato et al., 2000; Parent and Parent 2007; Koshimizu et al., 2013). Therefore,
419 we modified the network model parameters to test if the model without STN-STN connections
420 is also able to capture the behaviorally relevant dynamics of the LFP beta oscillations. Indeed,
421 with slight modifications of parameters (see Methods), all key results, including the time course of
422 beta around the time of movement preparation and execution (Figure 8A), the beta phase reset
423 (Figures 8B, C), and the complex relationship between beta and reaction time (Figures 8D, E),
424 were reproduced. This demonstrates that our model account of transient beta oscillations does
425 not depend on STN-STN recurrent connectivity.

426 In summary, our results show that the combination of 1) sensory responses of STN neurons,
427 2) movement-related inhibition of GPe neurons, and 3) ramping activity in STN, account for the
428 complex properties of beta power modulation over time, beta phase reset and correlations with
429 reaction time of rat electrophysiological recordings in the basal ganglia. Thereby, the model allows
430 us to make clear predictions about the underlying mechanisms and provides the basis for studying
431 functional consequences on neural processing and behavior.

432 Discussion

433 Oscillations in the LFP often reflect sensory, cognitive and motor aspects of neural processing,
434 but we lack understanding of how and why network oscillations emerge. Furthermore, we face
435 a gap between firing patterns of single neurons and network dynamics. Here we addressed this
436 by combining experimental data with computational modeling to study how firing patterns in
437 single units of task-performing healthy rats affect basal ganglia network dynamics. Although our
438 computational model was originally used to describe beta oscillations in Parkinson’s disease, this
439 model also accounted for properties of beta in healthy animals. Thereby, we characterize potential

440 neuronal mechanisms underlying oscillations, relate healthy to pathological beta oscillations, and
441 provide avenues for studying functional roles of beta in behavior.

442 **Neuronal mechanisms of beta oscillations**

443 Computational and experimental studies have implicated the STN-GPe network in beta oscil-
444 lations in Parkinson’s disease (Brown et al., 2001; Magill et al., 2001; Terman et al., 2002; Bevan
445 et al., 2002; Rubin and Terman, 2004; Brown and Williams, 2005; Mallet et al., 2008a; Tachibana
446 et al., 2011; Stein and Bar-Gad, 2013; Nevado-Holgado et al., 2014; Pavlides et al., 2015; Wei
447 et al., 2015). Moreover, cortico-subthalamic excitation as well as striato-pallidal inhibition can
448 generate beta oscillations in network models of the subthalamo-pallidal loop (Gillis et al., 2002;
449 Kumar et al., 2011; Nevado-Holgado et al., 2014; Pavlides et al., 2015; Wei et al., 2015; Ahn et
450 al., 2016). Consistently, we show that temporally regulated subthalamic excitation and pallidal
451 inhibition reproduces the dynamics of transient beta oscillations observed in the healthy basal
452 ganglia during behavior. Therefore, the same network that is responsible for beta oscillations in
453 Parkinson’s disease may also be involved in the generation of healthy beta.

454 As an alternative to the STN-GPe network, striatal MSNs (McCarthy et al., 2011), feedback
455 projections from GPe back to striatum (Corbit et al., 2016), or spread of cortical beta to STN
456 may be involved in basal ganglia beta oscillations. However, our model supports the role of the
457 STN-GPe network due to the close correspondence between single unit activity and the resulting
458 complex time course of beta oscillations. Whether other models for the generation of beta would
459 be able to account for the complex time course and behavioral correlates of beta remains to be
460 shown. While increased striatal spiking increases beta oscillations in several models (McCarthy
461 et al., 2011; Kumar et al., 2011; Corbit et al., 2016), our model emphasizes the role of excitatory
462 inputs to STN for the transient dynamics of beta oscillations. Overall, as beta oscillations are a
463 heterogeneous phenomenon (Szurhaj et al., 2003; Kilavik et al., 2012; Feingold et al., 2015), cortical
464 and subcortical circuit may contain several mechanisms for the generation of beta, e.g. to permit
465 long range communication (Fries, 2005). Therefore, these models are not necessarily exclusive and
466 a key future challenge will be to disentangle the different circuits and their interaction. Nonetheless
467 we have shown that the STN-GPe network is sufficient to explain many features of beta oscillations
468 in awake behaving animals.

469 **Direct and indirect pathway MSNs**

470 Activity of direct pathway MSNs (striato-nigral) promote actions, while indirect pathway MSNs
471 (striato-pallidal) suppress actions (Albin et al., 1989; Alexander and Crutcher, 1990; Kravitz et al.,
472 2010; Freeze et al., 2013; Roseberry et al., 2016). Here we considered movement-related increases
473 in MSN activity (Figure 1E) as inhibitory input to the model GPe (Figures 3A, B), without
474 knowing whether the recorded MSNs are part of the direct or indirect pathway. This assumption
475 is supported by evidence that direct and indirect pathway MSNs are concomitantly active during
476 movements (Cui et al., 2013; Isomura et al., 2013). Nevertheless, there might be important
477 activity differences between direct and indirect pathway neurons coordinating behavior. Whether
478 co-activation of indirect pathway MSNs during movement reflects the suppression of alternative
479 actions (Hikosaka et al., 2006; Redgrave et al., 2010) or activates specific neural assemblies in
480 motor cortex (Oldenburg and Sabatini, 2015) remains unclear. Furthermore, almost 60% of direct

481 pathway MSNs, possess collateral terminal fields in GPe (Cazorla et al., 2014). Therefore, during
482 movements GPe likely receives increased inhibitory input from striatal MSNs as incorporated in
483 the model.

484 **STN as a brake**

485 We found ramps in the activity of STN units while the animal was waiting for the Go cue.
486 During this time the animal has to prevent premature movements to receive the food reward.
487 Building on “hold-your-horses” models of STN (Frank, 2006), these ramps might prevent or delay
488 movements. Correspondingly, in our experimental data the ramps reached a plateau after the
489 Go cue, which was linked to the reaction time (i.e. the plateau persisted longer in trials with a
490 long reaction time; Figure 2A, bottom). Therefore, these ramps might modulate the readiness for
491 movement initiation. However, we also observed (data not shown) that the population activity of
492 the STN ramps did typically last until movement initiation, indicating that the offset of this STN
493 ramp does not provide a motor command itself. Instead, high STN activity might ensure that only
494 coordinated movement commands (potentially signaled by striatal output), but not premature
495 movement impulses, lead to motor output.

496 Conceptually, our model provides an important link between putative “hold-your-horses” ramp-
497 ing activity in STN, beta oscillations and reaction times. The ramping activity increased spiking
498 activity of the STN neurons and, consequently, lead to also more beta oscillations in the model
499 (Kumar et al., 2011). This was key in accounting for the bimodal shape of the mean beta power
500 for long reaction time trials (Figure 6B).

501 The STN ramps might be due to cortical drive. For example, in the motor cortex of mon-
502 keys ramping activity has been observed while the animals anticipated sensory cues and needed
503 to prevent premature movements (Confais et al., 2012). Furthermore, other cortical areas includ-
504 ing right inferior frontal cortex and the pre-supplemental motor area project to STN and have
505 been implicated in motor suppression (Wessel and Aron, 2017). In general, cortico-subthalamic
506 excitation has previously been proposed to be important for the generation of beta oscillations
507 (Tachibana et al., 2011; Pavlides et al., 2015). Importantly, the STN ramps during the hold period
508 increased the probability of transient beta in our model. This fits well with anti-kinetic aspects of
509 beta (Brown and Williams, 2005), and with STN activity correlating with slowness of movement
510 observed during the progression of Parkinson’s disease (Bergman et al., 1994; Remple et al., 2011).

511

512 **Behavioral relevance and predictions**

513 Beta oscillations seem to comprise a heterogeneous phenomenon with potentially different func-
514 tions and mechanisms depending on the brain region (Szurhaj et al., 2003; Kilavik et al., 2011;
515 Feingold et al., 2015). Here we extend this view by proposing that transient, non-pathological
516 basal ganglia beta can be driven by two distinct inputs. Firstly, beta oscillations were driven
517 by excitatory inputs to STN, including the ramping activity that might be linked to preventing
518 premature movements. Secondly, beta oscillations were also driven by striato-pallidal inhibition
519 during movement. Therefore, our model provides an explanation for why beta in some cases can
520 be “antikinetic” (Brown and Williams, 2005), but in other cases can also appear during movement

521 (Leventhal et al., 2012). Whether and how these two modes of beta make different functional
522 contributions, e.g. by differential communication with other brain regions (Fries, 2005), is an open
523 question.

524 Based on our model we make several experimentally testable predictions. Firstly, the two modes
525 of beta generation, via GPe inhibition and STN excitation, might have different signatures in LFP
526 recordings. If the beta is generated by GPe inhibition, the oscillation begins with a decrease in
527 GPe activity. If beta is generated by STN excitation, the beta oscillation begins with an increase in
528 STN. Although we do not know yet how spiking in the STN and GPe relates to patterns in the LFP,
529 these two modes could translate into different onset phases of beta. Therefore, we presume that
530 transient beta oscillations could be classified based on their onset phase, and that this is indicative
531 of whether the oscillation was driven by input to GPe or STN. Despite practical challenges, such
532 as detecting the exact onset phases of beta in noisy LFPs, this might provide valuable insights
533 into whether the two modes of beta generation have distinct behavioral correlates.

534 Secondly, our model makes specific predictions about the relation between activity of MSNs
535 projecting to GPe and the timing of beta oscillations (McCarthy et al., 2011). In recordings of
536 identified direct and indirect pathway MSNs, our model predicts that the activity of the D2 MSNs
537 predicts the timing of beta more accurately than the activity of the D1 MSNs. One complicating
538 factor is that this distinction does not apply to beta driven by cortical excitation of STN.

539 Another model prediction arises from our observation that the duration of excitatory inputs
540 to STN determines whether a phase reset occurs in the LFP or not. Sensory neuronal responses
541 (Figures 1C, D) are typically brief. We propose that sensory cues from other modalities have the
542 same effect, so that e.g. visual cues that lead to brief excitations of STN also lead to a phase reset
543 in the LFP signal. Furthermore, in addition to sensory cues, brief optogenetic stimulation of STN
544 might yield the same effect. Whether these cue-induced beta phase resets play also a functional
545 role, e.g. in the temporal coordination with inputs from other regions, remains to be shown.

546 Finally, we predict that changes in the structure of the STN ramping activity affects the prob-
547 ability of beta oscillations. If the STN ramps indeed reflect a “hold your horses” signal (Frank,
548 2006), changes in the behavioral paradigm that manipulate the readiness for movement initiation
549 should directly affect the ramping activity. For example, if the cost for the animal of a premature
550 response is increased, the corresponding ramping activity might change its time course and ampli-
551 tude. In the model this would directly translate into changes in the time course and probability
552 of transient beta.

553 In conclusion, the direct combination of our computational model with experimental data pro-
554 vides a connection between single unit activity and network oscillations. This helps us to study the
555 functional contributions of transient beta oscillation during sensorimotor processing in a behavioral
556 context.

References

- Ahn S, Zuber SE, Worth RM, and Rubchinsky LL (2016) Synchronized Beta-Band Oscillations in a Model of the Globus Pallidus-Subthalamic Nucleus Network under External Input. *Front Comput Neurosci* 10:134.
- Albin RL, Young AB, and Penney JB (1989) The functional anatomy of basal ganglia disorders. *Trends Neurosci* 12:366-375.
- Alegre M, Alonso-Frech F, Rodriguez-Oroz MC, Guridi J, Zamarbide I, Valencia, M, Manrique M, Obeso JA, and Artieda J (2005) Movement-related changes in oscillatory activity in the human subthalamic nucleus: ipsilateral vs. contralateral movements. *Eur J Neurosci*. 22:2315-2324.
- Alexander GE, Crutcher MD (1990) Functional architecture of basal ganglia circuits: neural substrates of parallel processing. *Trends Neurosci* 13:266-271.
- Anderson TW (2003) *An Introduction to Multivariate Statistical Analysis*, 3rd Edition. Wiley and Sons, New York, NY.
- Baker SN, Olivier E, and Lemon RN (1997) Coherent oscillations in monkey motor cortex and hand muscle EMG show task-dependent modulation. *J Physiol* 501:225-241.
- Bergman H, Wichmann T, Karmon B, and DeLong MR (1994) The primate subthalamic nucleus. II. Neuronal activity in the MPTP model of parkinsonism. *J Neurophysiol* 72:507-520.
- Berke JD, Okatan M, Skurski J, Eichenbaum HB (2004) Oscillatory entrainment of striatal neurons in freely moving rats. *Neuron* 43:883-896.
- Bevan MD, Bolam JP, Crossman AR (1994) Convergent synaptic input from the neostriatum and the subthalamus onto identified nigrothalamic neurons in the rat. *Eur J Neurosci* 6:320-334.
- Bevan MD, Magill PJ, Terman D, Bolam JP, Wilson CJ (2002) Move to the rhythm: oscillations in the subthalamic nucleus-external globus pallidus network. *Trends Neurosci* 25:525-31.
- Bishop GH (1936) The interpretation of cortical potentials. *Cold Spring Harbor Symp. Quant. Biol* 4:305-319.
- Brown P, Oliviero A, Mazzone P, Insola A, Tonali P, and Di Lazzaro V (2001) Dopamine dependency of oscillations between subthalamic nucleus and pallidum in Parkinson's disease. *J Neurosci* 21:1033-1038.
- Brown P (2007) Abnormal oscillatory synchronisation in the motor system leads to impaired movement. *Curr Opin Neurobiol* 17:656-664.
- Brown P, Williams D (2005) Basal ganglia local field potential activity: character and functional significance in the human. *Clin Neurophysiol* 116:2510-2519
- Brunel N (2000). Dynamics of sparsely connected networks of excitatory and inhibitory spiking neurons. *J Comput Neurosci* 8:183-208.
- Cassidy M, Mazzone P, Oliviero A, Insola A, Tonali P, Di Lazzaro V, Brown P (2002) Movement-related changes in synchronization in the human basal ganglia. *Brain* 125:1235-1246.
- Cazorla M, De Carvalho FD, Chohan MO, Shegda M, Chuhma N, Rayport S, Ahmari SE, Moore H, Kellendonk C (2014) Dopamine D2 receptors regulate the anatomical and functional balance of basal ganglia circuitry. *Neuron* 81:153-164.
- Chen CC, Litvak V, Gilbertson T, Kuhn A, Lu CS, Lee ST, Tsai CH, Tisch S, Limousin P, Hariz M, and Brown P (2007) Excessive synchronization of basal ganglia neurons at 20 Hz slows movement in Parkinsons disease. *Exp Neurol* 205:214-221.
- Confais J, Kilavik BE, Ponce-Alvarez A, Riehle A (2012) On the Anticipatory Precue Activity in Motor Cortex. *J Neurosci* 32:15359-15368.
- Corbit VL, Whalen TC, Zitelli KT, Crilly SY, Rubin JE, Gittis AH (2016) Pallidostriatal Projections Promote β Oscillations in a Dopamine-Depleted Biophysical Network Model. *J Neurosci* 36:5556-5571.

604 Courtemanche R, Fujii N, Graybiel AM (2003) Synchronous, focally modulated beta-band os-
605 cillations characterize local field potential activity in the striatum of awake behaving monkeys. *J*
606 *Neurosci* 23:11741-11752.

607 Creutzfeldt O, Watanabe S, Lux HD (1966a) Relation between EEG phenomena and potentials
608 of single cortical cells. I. Evoked responses after thalamic and epicortical stimulation. *Electroen-*
609 *cephalogr Clin Neurophysiol* 20:1-18.

610 Creutzfeldt O, Watanabe S, Lux HD (1966b) Relation between EEG phenomena and poten-
611 tials of single cortical cells. II. Spontaneous and convulsoid activity. *Electroencephalogr Clin*
612 *Neurophysiol* 20:19-37.

613 Cui G, Jun SB, Jin X, Pham MD, Vogel SS, Lovinger DM, and Costa RM (2013) Concurrent
614 activation of striatal direct and indirect pathways during action initiation. *Nature* 494:238-242.

615 Delong MR (1990) Primate models of movement disorders of basal ganglia origin. *Trends*
616 *Neurosci* 13:281-285.

617 Dodson PD, Larvin JT, Duffell JM, Garas FN, Doig NM, Kessarar N, Duguid IC, Bogacz R,
618 Butt SJ, Magill PJ (2015) Distinct developmental origins manifest in the specialized encoding of
619 movement by adult neurons of the external globus pallidus. *Neuron* 86:501-513.

620 Eccles JC (1951) Interpretation of action potentials evoked in the cerebral cortex. *J Neuro-*
621 *physiol* 3:339-464.

622 Engel AK, Fries P (2010) Beta-band oscillations: signalling the status quo? *Curr Opin Neurobiol*
623 20:156-165.

624 Feingold J, Gibson DJ, DePasquale B, Graybiel AM (2015) Bursts of beta oscillation differenti-
625 ate postperformance activity in the striatum and motor cortex of monkeys performing movement
626 tasks. *PNAS* 112:13687-13692.

627 Frank MJ (2006) Hold your horses: a dynamic computational role for the subthalamic nucleus
628 in decision making. *Neural Netw* 19:1120-1136.

629 Fries P (2005) A mechanism for cognitive dynamics: neuronal communication through neuronal
630 coherence. *Trends Cogn Sci* 9:474-480

631 Freeze BS, Kravitz AV, Hammack N, Berke JD, Kreitzer AC (2013) Control of basal ganglia
632 output by direct and indirect pathway projection neurons. *J Neurosci* 33:18531-18539.

633 Gage GJ, Stoetzner CR, Wiltschko AB, and Berke JD (2010) Selective activation of striatal
634 fast-spiking interneurons during choice execution. *Neuron* 67:466-479.

635 Gewaltig M-O, Diesmann M (2007) NEST (Neural Simulation Tool) *Scholarpedia* 2(4):1430.

636 Gillis A, Willshaw D, Li Z (2002) Subthalamic-pallidal interactions are critical in determining
637 normal and abnormal functioning of the basal ganglia. *Proc Biol Sci* 269:545-551.

638 Gillbertson T, Lalo E, Doyle L, Di Lazzaro V, Cioni B, and Brown P (2005) Existing motor
639 state is favored at the expenses of new movement during 13-35 Hz oscillatory synchrony in the
640 human corticospinal system. *J Neurosci* 25:7771-7779.

641 Hammond C, Bergman H, and Brown P (2007) Pathological synchronization in Parkinson's
642 disease: networks, models and treatments. *Trends Neurosci* 30:357-366.

643 Hammond C, and Yelnik J (1983) Intracellular labelling of rat subthalamic neurones with
644 horseradish peroxidase: computer analysis of dendrites and characterization of axon arborization.
645 *Neuroscience* 8:781-790.

646 Hikoska O, Nakamura K, Nakamuran H (2006) Basal ganglia orient eyes to reward. *J Neuro-*
647 *physiol* 95:567-584.

648 Isomura Y, Takekawa T, Harukuni R, Handa T, Aizawa H, Takada M, and Fuki T (1023)
649 Reward-modulated motor information in identified striatum neurons. *J Neurosci* 33:10209-10220.

650 Jensen O, Goel P, Kopell N, Pohja M, Hari R, Ermentrout B (2005) On the human sensorimotor-
651 cortex beta rhythm: sources and modeling. *NeuroImage* 26:347-355.

652 Kilavik BE, Ponce-Alvarez A, Trachel R, Confais J, Takerkart S, Riehle A (2012) Context-
653 related frequency modulations of macaque motor cortical LFP beta oscillations. *Cereb Cortex*
654 22:2148-2159.

655 Kitai ST, Kita H (1987) Anatomy and physiology of the subthalamic nucleus: a driving force
656 of the basal ganglia. In: *The basal ganglia II: structure and function; current concepts* (Carpenter
657 MB, Jayaraman A, eds), pp. 357-373. New York: Plenum.

658 Klee MR, Offenloch K, Tigges J (1965) Cross-correlation analysis of electroencephalographic
659 potentials and slow membrane transients. *Science* 147:519-521.

660 Kravitz AV, Freeze BS, Parker PRL, Kay K, Thwin MT, Deisseroth K, Kreitzer AC (2010)
661 Regulation of parkinsonian motor behaviours by optogenetic control of basal ganglia circuitry.
662 *Nature* 466:622-626.

663 Kuhn AA, Williams D, Kupsch A, Limousin P, Hariz M, Schneider GH, Yarrow K, and Brown P
664 (2004) Event-related beta desynchronization in human subthalamic nucleus correlates with motor
665 performance. *Brain* 127:735-746.

666 Kuhn AA, Kupsch A, Schneider GH, Brown P (2006) Reduction in subthalamic 8-35 Hz os-
667 cillatory activity correlates with clinical improvement in Parkinson's disease. *Eur J Neurosci*
668 23:1956-1960.

669 Kumar A, Cardanobile S, Rotter S, and Aersten A (2011) The role of inhibition in generation
670 and controlling Parkinson's disease oscillations in the basal ganglia. *Front Syst Neurosci* 5:86.

671 Koshimizu Y, Fujiyama F, Nakamura KC, Furuta T, Kaneko T (2013) Quantitative analysis of
672 axon bouton distribution of subthalamic nucleus neurons in the rat by single neuron visualization
673 with a viral vector. *J Comp Neurol* 521:2125-2146.

674 Leventhal DK, Gage GJ, Schmidt R, Pettibone JR, Case AC, and Berke JD (2012) Basal ganglia
675 beta oscillations accompany cue utilization. *Neuron* 73:523-536.

676 Levy R, Ashby P, Hutchison W.D, Lang A.E, Lozano A.M, and Dostrovsky J.O (2002) De-
677 pendence of subthalamic nucleus oscillations on movement and dopamine in Parkinson's disease.
678 *Brain* 125:1196-1209.

679 Little S, Pogosyan A, Kuhn AA, and Brown P (2012) band stability over time correlates with
680 Parkinsonian rigidity and bradykinesia. *Exp Neurol* 236:383-388.

681 MacKay WA, and Mendonca AJ (1995) Field potential oscillatory bursts in parietal cortex
682 before and during reach. *Brain Res* 704:167-174.

683 Magill PJ, Bolam JP, Bevan MD (2001) Dopamine regulates the impact of the cerebral cortex
684 on the subthalamic nucleus-globus pallidus network. *Neuroscience* 106:313-330

685 Mallet N, Pogosyan A, Marton LF, Bolam JP, Brown P, Magill PJ (2008) Parkinsonian beta
686 oscillations in the external globus pallidus and their relationship with subthalamic nucleus activity.
687 *J Neurosci* 28:14245-14258.

688 Mallet N, Schmidt R, Leventhal D, Chen F, Amer N, Boraud T (2016) Arkypallidal Cells Send
689 a Stop Signal to Striatum. *Neuron* 89:308-316

690 McCarthy MM, Moore-Kochlacs C, Gu X, Boyden ES, Han X, Kopell N (2011) Striatal origin
691 of the pathologic beta oscillations in Parkinson's disease. *PNAS* 108:11620-11625.

692 Nevado-Holgado AJ, Mallet N, Magill PJ, Bogacz R (2014) Effective connectivity of the sub-
693 thalamic nucleus-globus pallidus network during Parkinsonian oscillations. *Journal of physiology*
694 7:1429-1455.

695 Niedermeyer E, Lopes da Silva F (1998) *Electroencephalography* (4th edition), Williams and
696 Wilkins, Baltimore.

697 Nunez PL, Srinivasan R (2005) *Electric Fields of the Brain*. Oxford university press, Oxford,
698 UK.

699 Oldenburg IA, Sabatini BL (2015) Antagonistic but not symmetric regulation of primary motor

700 cortex by basal ganglia direct and indirect pathways. *Neuron* 86:1174-1181.

701 Pan WX, Hyland BI (2005) Pedunculopontine tegmental nucleus controls conditioned responses
702 of midbrain dopamine neurons in behaving rats. *J Neurosci* 25:4725-4732.

703 Parent M, Parent A (2007) The microcircuitry of primate subthalamic nucleus. *Parkinsonism*
704 *& Related Disorders* 13:S292-S295.

705 Parent A, Hazrati LN (1995) Functional anatomy of the basal ganglia. I. The cortico-basal
706 ganglia-thalamo-cortical loop. *Brain Res Rev* 20:91-127.

707 Pavlides A, Hogan SJ, Bogacz R (2015) Computational models describing possible mechanisms
708 for generation of excessive beta oscillations in Parkinson's disease. *PLoS Comput Biol* 11:12.

709 Pfurtscheller G, Stancak A. Jr, and Neuper C (1996) Post-movement beta synchronization. A
710 correlate of an idling motor area? *Electroencephalogr. Clin Neurophysiol* 98:281-293.

711 Pfurtscheller G, Graimann B, Huggins JE, Levine SP, and Schuh LA (2003) Spatiotemporal
712 patterns of beta desynchronization and gamma synchronization in corticographic data during self-
713 paced movement. *Clin Neurophysiol* 114:1226-1236.

714 Plenz D, Kital ST (1999) A basal ganglia pacemaker formed by the subthalamic nucleus and
715 external globus pallidus. *Nature* 400:677-682

716 Pogosyan A, Gaynor LD, Eusebio A, and Brown P (2009) Boosting cortical activity at Beta-
717 band frequencies slows movement in humans. *Curr Biol* 19:1637-1641.

718 Raz A, Vaadia E, and Bergman H (2000) Firing patterns and correlations of spontaneous dis-
719 charge of pallidal neurons in the normal and the tremulous 1-methyl-4-phenyl- 1,2,3,6-tetrahydropyridine
720 vervet model of parkinsonism. *J Neurosci* 20:8559-8571.

721 Redgrave P, Rodriguez M, Smith Y, Rodriguez-Oroz MC, Lehericy S, Bergman H, Agid Y,
722 DeLong MR, Obeso JA (2010) Goal-directed and habitual control in the basal ganglia: implications
723 for Parkinson's disease. *Nat Rev Neurosci* 11:760-772.

724 Remple MS, Bradenham CH, Kao CC, Charles PD, Neimat JS, Konard PE (2011) Subthalamic
725 nucleus neuronal firing rate increases with Parkinson's disease progression. *Mov Disord* 26:1657-
726 1662.

727 Roseberry TK, Lee AM, Lalive AL, Wilbrecht L, Bonci A, Kreitzer AC (2016) Cell-type-specific
728 control of brainstem locomotor circuits by basal ganglia. *Cell* 164:526-537.

729 Sato F, Parent M, Levesque M, and Parent A (2000) Axonal branching pattern of neurons of
730 the subthalamic nucleus in primates. *J Comp Neurol* 424:142-152.

731 Schmidt R, Leventhal DK, Mallet N, Chen F, Berke JD (2013) Canceling actions involves a
732 race between basal ganglia pathways. *Nat Neurosci* 16:1118-1124.

733 Shink E, Bevan MD, Bolam JP, Smith Y (1996) The subthalamic nucleus and the external
734 pallidum: two tightly interconnected structures that control the output of the basal ganglia in the
735 monkey. *Neuroscience* 73:335-357.

736 Smith Y, Hazrati LN, Parent A (1990) Efferent projections of the subthalamic nucleus in the
737 squirrel monkey as studied by the PHA-L anterograde tracing method. *J Comp Neurol* 294:306-
738 323.

739 Sochurkova D, Rektor I (2003) Event-related desynchronization/synchronization in the puta-
740 men. An SEEG case study. *Exp Brain Res* 149:401-404.

741 Swann N, Tandon N, Canolty R, Ellmore TM, McEvoy LK, Dreyer S, DiSano M, and Aron AR
742 (2009) Intracranial EEG reveals a time- and frequency-specific role for the right inferior frontal
743 gyrus and primary motor cortex in stopping initiated responses. *J Neurosci* 29:12675-12685.

744 Szurhaj W, Derambure P, Labyt E, Cassim F, Bourriez JL, Isnard J, Guieu JD, Mauguiere F
745 (2003) Basic mechanisms of central rhythms reactivity to preparation and execution of a voluntary
746 movement: a stereoelectroencephalographic study. *Clin Neurophysiol* 114:107-119.

747 Tachibana Y, Iwamuro H, Kita H, Takada M, Nambu A (2011) Subthalamo-pallidal interactions

748 underlying parkinsonian neuronal oscillations in the primate basal ganglia. *Eur J Neurosci* 34:1470-
749 1484.

750 Tan H, Jenkinson N, Brown P (2014) Dynamic neural correlates of motor error monitoring and
751 adaptation during trial-to-trial learning. *J Neurosci* 34:5678-5688.

752 Terman D, Rubin JE, Yew AC, and Wilson CJ (2002) Activity patterns in a model for the
753 subthalamopallidal network of the basal ganglia. *J Neurosci* 22:2963-2976.

754 Wei W, Rubin JE, Wang XJ (2015) Role of the Indirect Pathway of the Basal Ganglia in
755 Perceptual Decision Making. *J Neurosci* 35:4052-4064.

756 Wessel JR, Aron AR (2017) On the Globality of Motor Suppression: Unexpected Events and
757 Their Influence on Behavior and Cognition. *Neuron* 93:259-280.

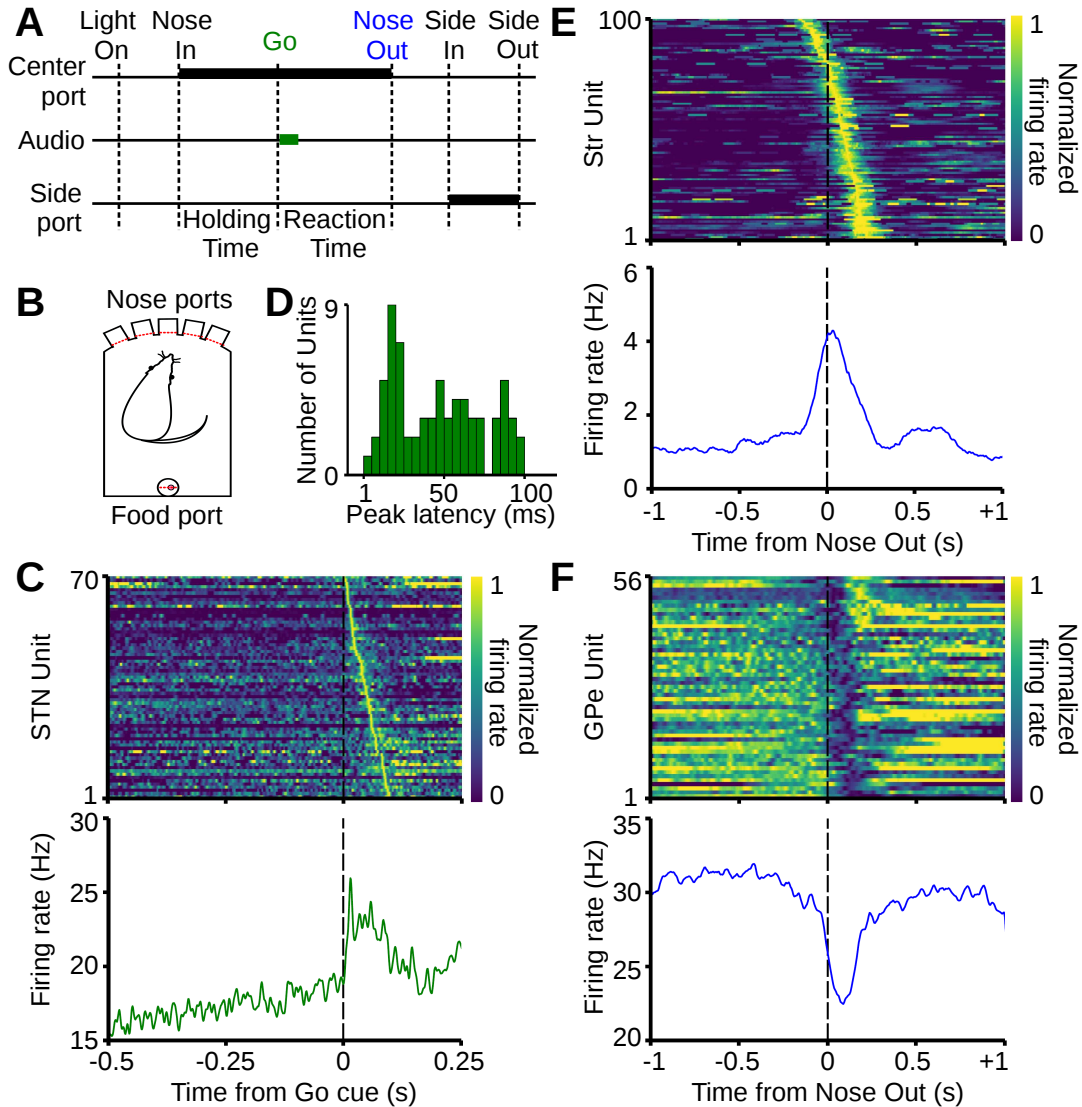


Figure 1: Single unit responses to sensory and motor events during performance of the behavioral task. **A**, Sequence of behavioral events during the experiment. Thick black bars show the position of the animal and thick green bar shows the occurrence of the sensory cue. Holding time refers to a random time delay (500 to 1200 ms) in which the animal waits in one of the three central ports for the sensory cue. Reaction time is measured as the time between the onset of the Go cue and movement initiation (Nose Out). **B**, Scheme of the operant chamber with five nose ports in front and a food port in the back. **C** (top) Normalized mean firing rates of single STN units responding to the Go cue with an increase in firing rate (sorted by peak latency; each row shows activity of one unit). Bottom, corresponding mean firing rate of the STN subpopulation. **D**, Distribution of peak latencies relative to the time of Go cue for STN neurons shown in C. **E** (top) Normalized firing rates of single units in the striatum (putative MSNs) increasing their activity around movement onset (sorted by time of peak activity). Bottom, corresponding mean firing rate of the subpopulation. **F**, Same as E, for GPe subpopulation decreasing activity around movement onset.

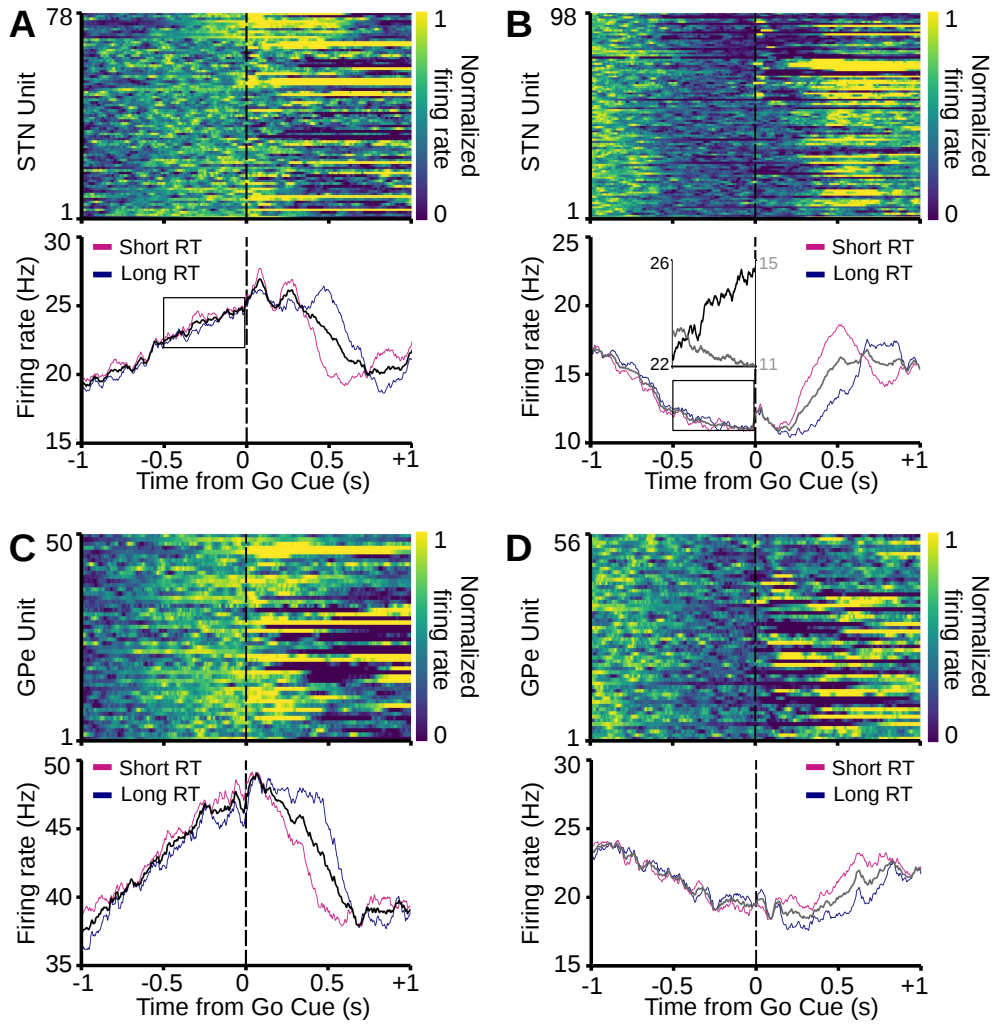


Figure 2: Ramping activity in STN and GPe while the animal is waiting for the Go cue. **A** (top) Normalized mean firing rate of single STN units with a positive ramp in firing rate before the Go cue. Bottom, corresponding mean firing rate of the STN subpopulation in all trials (black) and subsets of long (cyan) and short (magenta) reaction time trials. **B**, Same as A, for single STN units with a negative ramp in their firing rate before the Go cue. Inset, direct comparison between average firing rates of neurons in A, and B, corresponding to the areas inside the black rectangles. **C**, **D**, Similar to A and B, respectively, for GPe units.

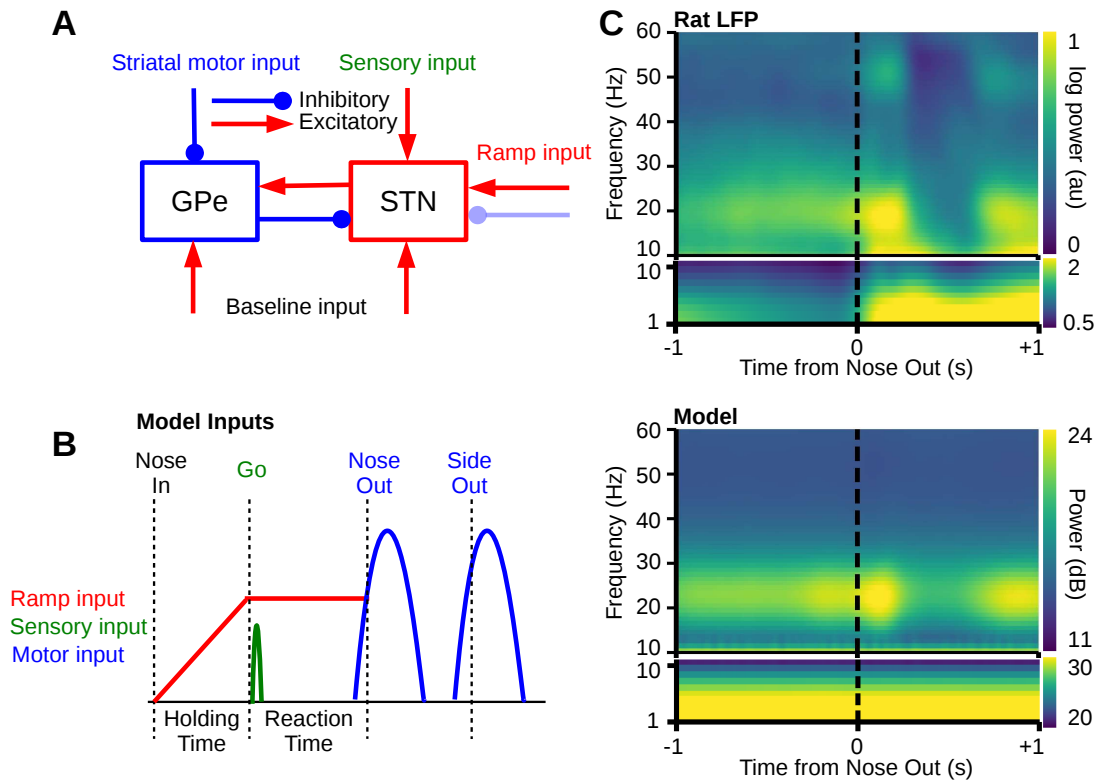


Figure 3: Computational model of beta oscillations stimulated with biologically realistic input patterns. **A**, Scheme of the STN-GPe spiking neuronal network model. Motor input is provided as striatal inhibitory input to the GPe whereas sensory input is provided as excitatory input to the STN. Ramp input comprises separate excitatory and inhibitory inputs to separate STN subpopulations (see Methods). **B**, Schematized temporal sequence of inputs to the network model during simulation of the behavioral task. **C** (top) Mean spectrogram of GPe LFP data showing modulation of LFP beta power during movement initiation. Bottom, Mean spectrogram (over 400 simulations) of GPe average firing rates for simulation of correct Go trials in the network model matching the time course of beta power in the experimental data.

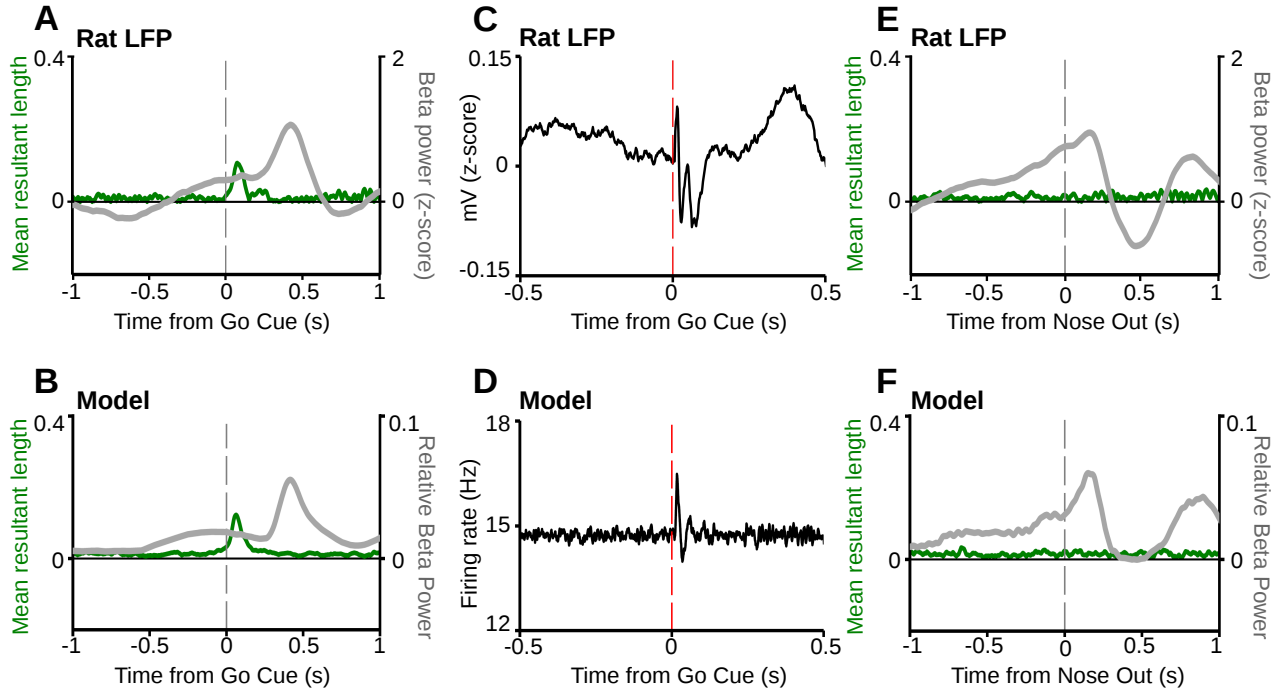


Figure 4: Sensory cues lead to a beta phase reset in both experimental data and in the network model. **A, B**, Time resolved beta mean resultant length (left axes, green) and beta power (right axes, gray) of GPe LFP data during correctly performed contralateral go trials averaged across all rats (**A**) and of the network model GPe population firing rate (**B**; average of 400 simulations). Note that sensory input is associated with a phase reset in both experimental data and in the model, shown as a brief increase in the value of the mean resultant length after the Go cue. **C**, Mean of the raw experimental STN LFP data, over all correctly performed contralateral go trials, aligned to the Go cue. **D**, Mean of the STN population firing rates in response to the Go cue in the network model (average of 400 simulations). **E, F**, The same analysis and simulations as in **A** and **B**, respectively, but aligned to movement onset. Note that the phase distribution is random during initiation and execution of movement in both the rat and the network model (no increase in the mean resultant length around movement onset).

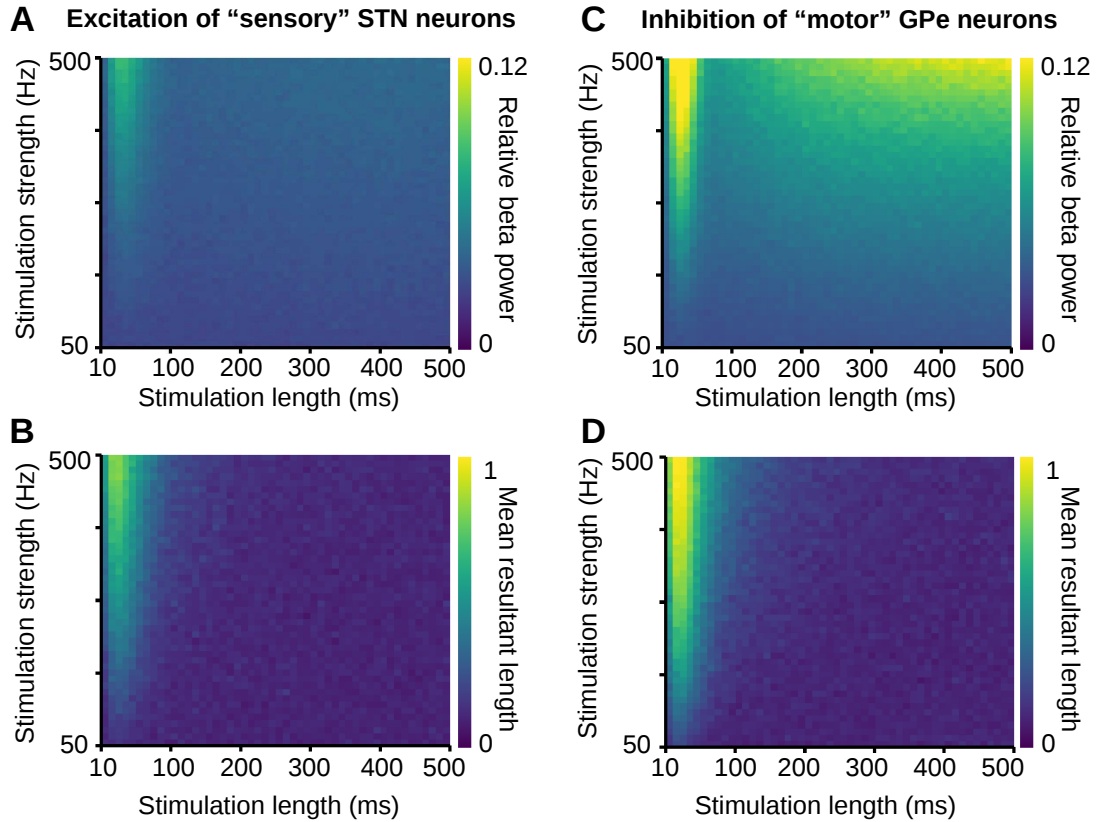


Figure 5: Effect of stimulation duration on beta power and phase reset in the network model. **A, B**, Relative beta power (A) and beta phase reset (B; measured by the mean resultant length) in the model GPe caused by excitatory input to the 30% "sensory" STN neurons of varying duration (x-axis) and strength (y-axis). **C, D**, Relative beta power (C) and phase reset (D) in the model GPe caused by inhibitory input to the 38% "motor" GPe neurons (see Methods) of varying duration (x-axis) and strength (y-axis). Note that in all panels we measure beta oscillations based on the GPe population firing rate.

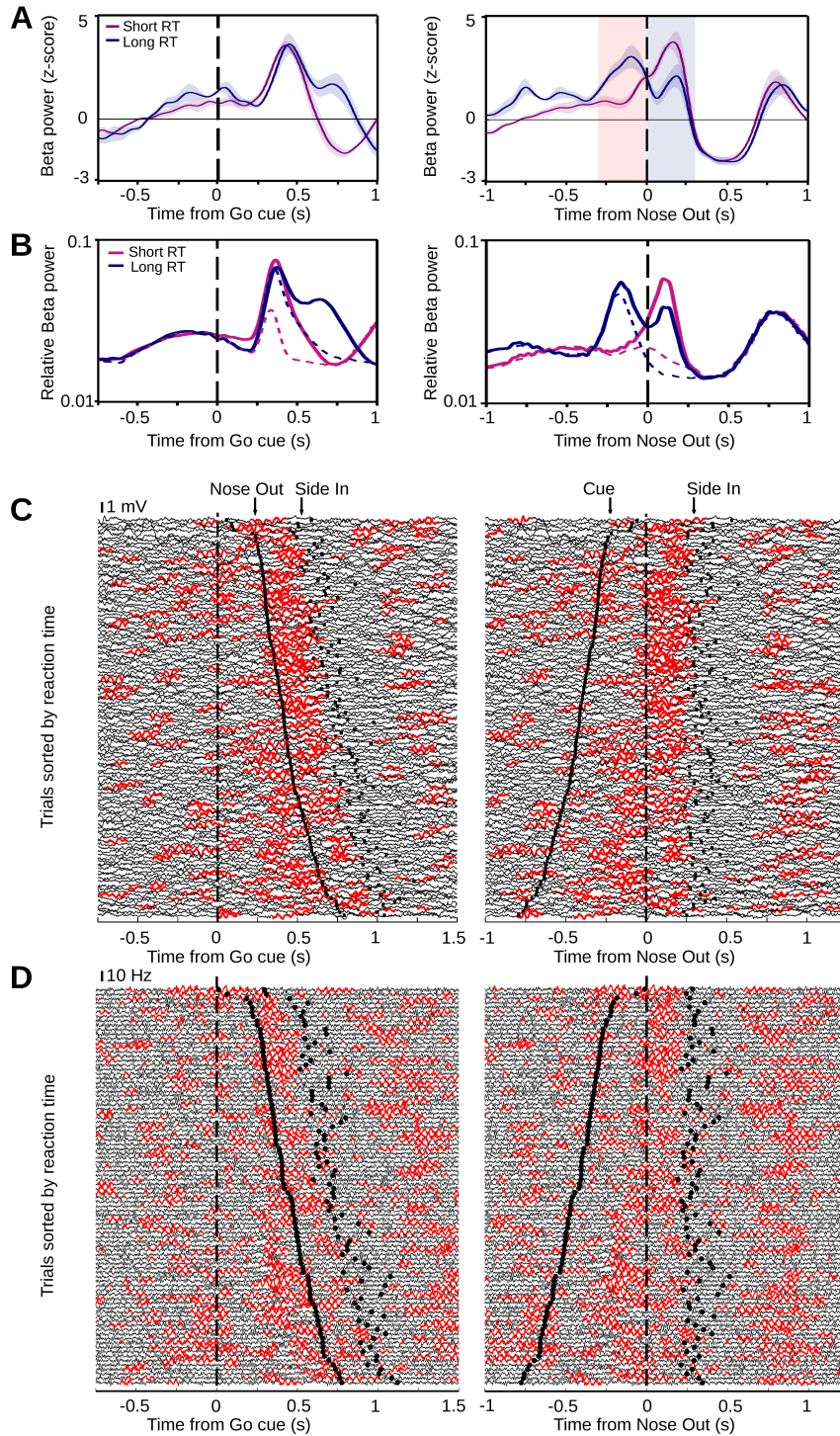


Figure 6: Relationship between beta oscillations and reaction time. **A**, Mean beta power of striatal LFP data for short (<500 ms) and long (>500 ms) reaction time trials aligned to the Go cue (left) and movement onset (right), averaged across rats (adapted from Leventhal et al., 2012, with permission from Elsevier). **B**, Mean relative beta power of GPe population firing rates in the network model (averaged over 400 simulations), exposed to ramp, sensory and motor stimulation patterns (solid lines). For comparison, if the striatal motor input to GPe is withheld in the model (dashed lines), the second beta peak disappears for long reaction time trials (see blue dashed line in right panel). **C**, Single-trial striatal LFP traces from a single recording session, sorted by reaction time, aligned to the Go cue (left) and movement onset (right) with beta epochs marked in red (adapted from Leventhal et al., 2012, with permission from Elsevier). **D**, Same visualization for single-trial model simulations with each trace showing the population firing rate of GPe neurons in the network model. For simulation of each trial, the model reaction time was randomly selected from the experimental data.

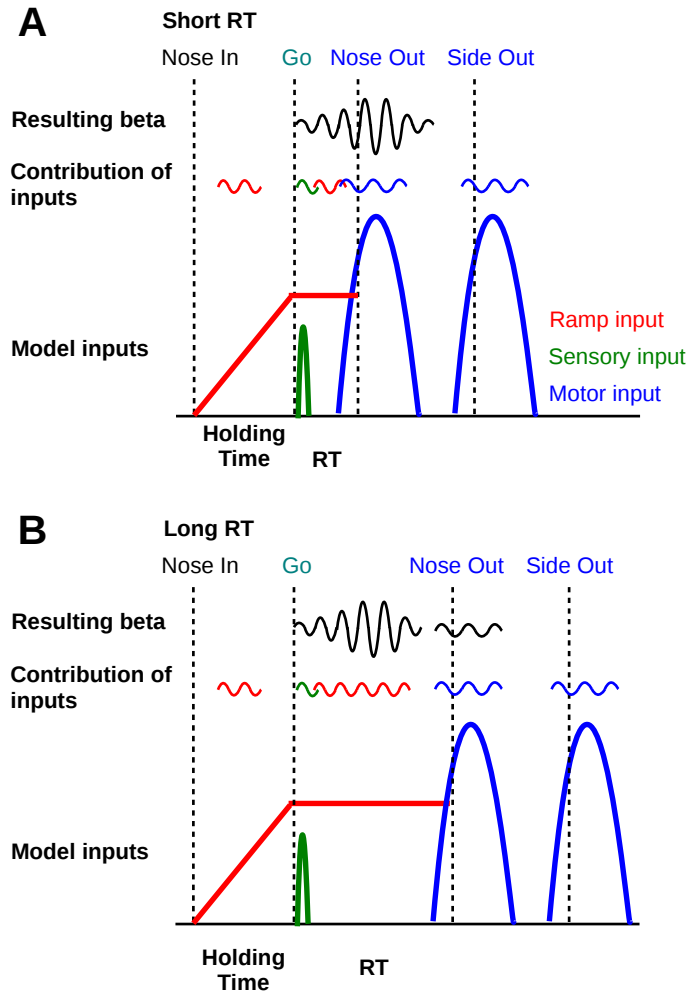


Figure 7: Scheme of contribution of each stimulation component to the generation of beta oscillations in short (A), and long (B) reaction time trials. Red, green, and blue schematized beta oscillations show the contribution of each individual input (ramp, sensory, and motor inputs, respectively) without the other one. Note that for short reaction time trials, interaction between beta oscillations due to ramp, sensory, and motor inputs leads to transient increase in beta power around the time of movement onset (black trace shows the net effect of the interaction). For long reaction time trials, interaction between beta oscillations due to sensory and ramp inputs leads to transient increase in beta power before the time of movement onset which is followed by another beta epoch due to motor input (black traces show the net effect of the interaction).

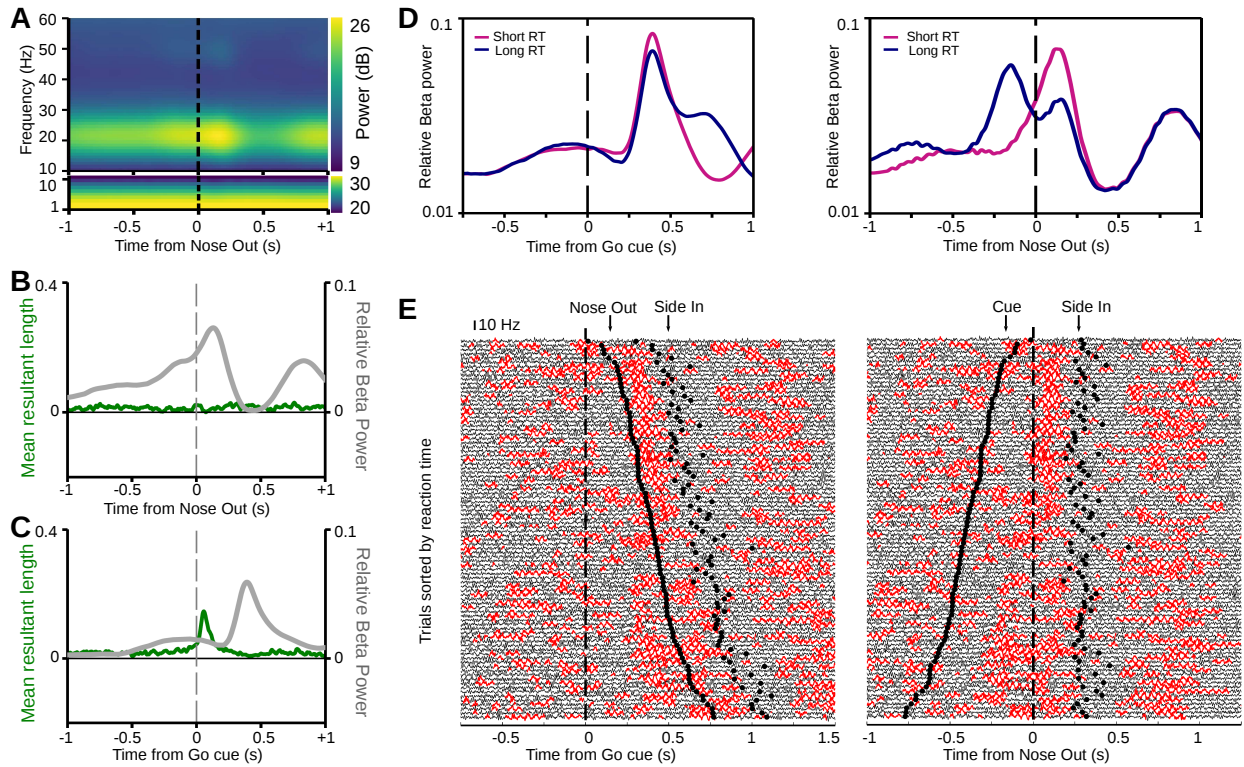


Figure 8: The network model without recurrent connections in STN reproduces all key results. **A**, Mean spectrogram (over 400 simulations) of GPe average firing rates for simulation of correct Go trials in the modified network model matching the time course of beta power in the experimental data. **B**, **C**, Time resolved beta mean resultant length (left axes, green) and beta power (right axes, gray) of the GPe population firing rate in the modified network model, aligned to the movement onset (**B**) and to the Go cue (**C**; average of 400 simulations). **D**, Mean relative beta power of GPe population firing rates in the modified network model aligned to the Go cue (left), and movement onset (right), averaged across 400 simulations. **E**, Single-trial simulations of the modified network model, sorted by reaction time, with each trace showing the population firing rate of GPe neurons, aligned to the Go cue (left) and movement onset (right; beta epochs are marked in red).